Check for updates

ADVANCED MATERIALS
www.advmat.de

Magnetic Putty as a Reconfigurable, Recyclable, and Accessible Soft Robotic Material

*Meng Li, Aniket Pal, Junghwan Byun, Gaurav Gardi, and Metin Sitti**

Magnetically hard materials are widely used to build soft magnetic robots, providing large magnetic force/torque and macrodomain programmability. However, their high magnetic coercivity often presents practical challenges when attempting to reconfigure magnetization patterns, requiring a large magnetic field or heating. In this study, magnetic putty is introduced as a magnetically hard and soft material with large remanence and low coercivity. It is shown that the magnetization of magnetic putty can be easily reoriented with maximum magnitude using an external field that is only one-tenth of its coercivity. Additionally, magnetic putty is a malleable, autonomous self-healing material that can be recycled and repurposed. The authors anticipate magnetic putty could provide a versatile and accessible tool for various magnetic robotics applications for fast prototyping and explorations for research and educational purposes.

1. Introduction

Soft-bodied robots that can be actuated and controlled remotely using various stimuli hold immense potential for applications in hard-to-reach and confined spaces.[1–4] Among various remote (wireless) stimuli, the magnetic field is widely explored due to its large penetration depth in biological tissues, high dexterity and speed, and large force/deformation controlled with high temporal resolution. Magnetically inert robotic bodies can be made magnetically responsive by attaching permanent magnets,[5,6] embedding electromagnetic coils,[7] incorporating magnetic particles,[8,9] or coating the surface with magnetic materials (metal, alloy, polymeric composites, etc.).[10–12] Alternatively, the soft body itself is (wholly or partially) constructed with magnetic composites.[13–15] The most widely used magnetic composites are polymeric matrices embedded with either magnetically soft or hard particles.[16] The former is easier to remagnetize, but it suffers from low remanence, that is, the magnetic torque/force is low when the external magnetic field is small. The latter—made with hard magnetic particles—requires a large reversal field to change the direction of its magnetization. Researchers have taken advantage of this large coercivity to fabricate shape-programmable soft structures with designed magnetic macrodomains.[14,17,18] The magnetization profile enables heterogeneous shape deformation upon the application of a uniform magnetic field. However, under certain circumstances, it is desirable to reprogram and reconfigure the robot to switch between different locomotion modalities and functionalities, especially when refabrication and retrieval of the robot is not trivial. The large fields needed to reverse the magnetization direction of hard-magnetic materials pose practical difficulties in reprogramming this type of magnetic soft robot.

Various strategies have been developed to address the reconfigurability of magnetic soft robots made with hard-magnetic particles. One can selectively reduce the particle coercivity in desired locations by laser-assisted heating; once the coercivity is lowered, one can apply a magnetic field exceeding the reduced coercivity (while still below the original coercivity) to only remagnetize the heated area and leave the rest intact.[19] Local heating can also induce selective matrix softening by phase change[20] or cleavage of chemical bonds.[21] This reduction of fixation allows the magnetized particles to reorient under external magnetic fields thus reconfiguring the magnetization direction of the heated area; once the composite cools down and hardens, the new orientation, and therefore the new magnetization direction, is locked in place. Normally, a strong magnetic field surpassing the particle coercivity or extra energy input, such as heat, or humidity,[12] is required to reprogram the magnetization of hard-magnetic materials.

M. Li[+], A. Pal[++], J. Byun, G. Gardi, M. Sitti
Department of Physical Intelligence
Max Planck Institute for Intelligent Systems
70569 Stuttgart, Germany
E-mail: aniket.pal@mib.uni-stuttgart.de; sitti@is.mpg.de
M. Sitti
Institute for Biomedical Engineering
ETH Zürich
Zürich 8092, Switzerland
M. Sitti
School of Medicine and College of Engineering
Koç University
Istanbul 34450, Turkey

The ORCID identification number(s) for the author(s) of this article can be found under https://doi.org/10.1002/adma.202304825

[+]Present address: Department of Civil and Environmental Engineering, Massachusetts Institute of Technology, Cambridge, MA 02139, USA

[++]Present address: Institute of Applied Mechanics, University of Stuttgart, 70569 Stuttgart, Germany

© 2023 The Authors. Advanced Materials published by Wiley-VCH GmbH. This is an open access article under the terms of the Creative Commons Attribution License, which permits use, distribution and reproduction in any medium, provided the original work is properly cited.

DOI: 10.1002/adma.202304825

15214095, 2023, 48, Downloaded from https://onlinelibrary.wiley.com/doi/10.1002/adma.202304825 by Koc University, Wiley Online Library on [26/02/2024]. See the Terms and Conditions (https://onlinelibrary.wiley.com/terms-and-conditions) on Wiley Online Library for rules of use; OA articles are governed by the applicable Creative Commons License

Besides material property reprogramming, geometrical reprogramming is also of great interest to the soft robotics community.[22] This could mean shape adaptation under external stimuli or self-healing, which enables robots to recover from mechanical failures[23,24] and allows the assembly of different modules into one entity. When shapes are changed, obstacles are passed,[25,26] locomotion modalities are changed,[27] and/or mechanical forces are exerted.[28] The capability of easily switching between arbitrary 3D geometries is desirable in terms of allowing the same material to be recycled and repurposed. However, this aspect of robotic material design is often overlooked.

Compared with traditional elastomeric magnetic composites with hard-magnetic particles and commercial magnetic putty, which is embedded with soft-magnetic particles, this work presents magnetic putty with hard-magnetic particles in a viscoelastic putty matrix as a new magnetic robot material (**Figure 1**A). The magnetic putty is easy to shape in 3D and can autonomously self-heal, allowing recovery from mechanical damage and assembly of parts without adhesives. The unbinding putty matrix allows the magnetic particles to stay mobile, giving the magnetic putty its unique magnetic properties. The magnetic putty combines the benefits of hard- and soft-magnetic materials—high remanence and low coercivity—having large magnetic force under small fields and an easily reconfigurable magnetization profile. We also quantify how its magnetic field-induced stress changes under alternating magnetic fields. We show that, at a low magnetic field frequency and large field magnitude, it becomes an analog frequency doubler. We demonstrate using magnetic putty as a robotic material to build reconfigurable magnetic setups, shapable magnets with adaptive polarities, recyclable magnetic robots, and growing bioinspired rotating vines. We envision that this easy-to-access material can provide the soft robotics community with a research and educational tool to explore fundamental questions and fast prototype novel magnetic soft robots.

2. Results and Discussion

2.1. Morphology, Composition, and Self-Healing

The putty is formed by partially crosslinking polydimethylsiloxane (PDMS) oligomers using boric acid (Figure 1B). Through polycondensation reactions,[29] the boron atoms can connect two or three PDMS oligomer chains[30] (Figure S1, Supporting Information). Also, coordinate bonds can form between the boron and the oxygen atom in the backbone of the neighboring chains.[30,31] Hydrogen bonds form between the pendant hydroxyl group of the boron atom and the adjacent hydroxyl groups and oligomers. These coordinate bonds and hydrogen bonds are dynamic; they can be broken and reformed both internally due to molecular thermal motion and polymer chain sliding and externally under mechanical deformation.

The addition of hard-magnetic particles (Neodymium-Iron-Boron, NdFeB, Figure 1C) to the pristine putty renders the composite magnetically responsive, thus we refer to it as magnetic putty. The magnetic particles are fully magnetized by placing the magnetic putty in a 1.8 T uniform magnetic field for five seconds. Without specific notation, all magnetic putty samples mentioned in this work are magnetized this way. With a permanent magnet, the magnetic force is strong enough to deform the putty and elongate it as if the putty were growing (Figure 1D, Movie S1, Supporting Information); after removing the magnet, the elongated form remains. The putty can be easily shaped into 3D geometries and largely maintain that geometry (e.g., a braided wreath as shown in Figure 1E).

The quick reformation of the dynamic bonds allows the magnetic putty to self-heal. By bringing two parts into contact, without any external intervention, such as heat, humidity, or magnetic fields, they become inseparable within a second (Figure 1F, Movie S2, Supporting Information). After 5 min rest, the healed piece did not show inferior performance compared with the uncut sample in tensile tests (Figure 1G, Figure S2, Supporting Information). This autonomous self-healing property enables quick and easy assembly of magnetic putty parts without using adhesives.

2.2. Rheological Properties: Viscoelasticity

Silly Putty is well-known for its interesting viscoelastic properties and the pristine putty in this work resembles its commercially available counterparts in composition. Many works have shown rheological characterizations of putty-like materials.[32–34] At a high deformation rate, the magnetic putty appears elastic as it bounces when one throws it against a rigid surface (Movie S3, Supporting Information). The same putty, however, if left alone, relaxes its shape over time, showing a viscous flow behavior (Figure 1H, Movie S4, Supporting Information). One can make the putty stiffer, thus maintaining its shape better by increasing the boric acid to PDMS ratio during the fabrication of pristine putty, which increases the crosslinking density of the polymeric network.[35] When compressed, the putty has a larger apparent compressive modulus under a faster compression speed (Figure S3, Supporting Information). For example, for the 50 wt.% magnetic sample, when compressed at a rate of 1 mm s^{-1}, the compressive modulus is 60 kPa, which is 14 kPa under 0.1 mm s^{-1}. After the deformation stops, the stress showed a dampened relaxation and reached zero within 10 s. (**Figure 2**A).

By characterizing the viscoelastic behavior of magnetic putty, we can learn how the added hard-magnetic particles affect its mechanical properties. For the amplitude-sweeping dynamic rheological measurements (Figure 2B), the linear viscoelastic region is the low-strain region where the storage modulus (G') and loss modulus (G'') are invariant to the increase of the strain amplitude (γ). The strain at which the storage modulus drops to 95% of its value in the linear region is defined as the critical strain, γ_c, marking the yield point when the putty starts to undergo plastic deformation. All putty samples have a critical strain below 0.3% with a decreasing trend as the particle loading increases (Figure S4A, Supporting Information). The low-critical strains corroborate the fact that these magnetic putties can be easily and permanently deformed. The yield stress (Figure S4A, Supporting Information), below which the putty can maintain its shape without flowing, is calculated by multiplying the complex shear modulus $\left(G^* = \sqrt{G'^2 + G''^2}\right)$ of the linear region with the critical strain, γ_c. It takes higher stress to initiate flow in putty with higher particle loadings thus those have better shape retention.

© 2023 The Authors. Advanced Materials published by Wiley-VCH GmbH

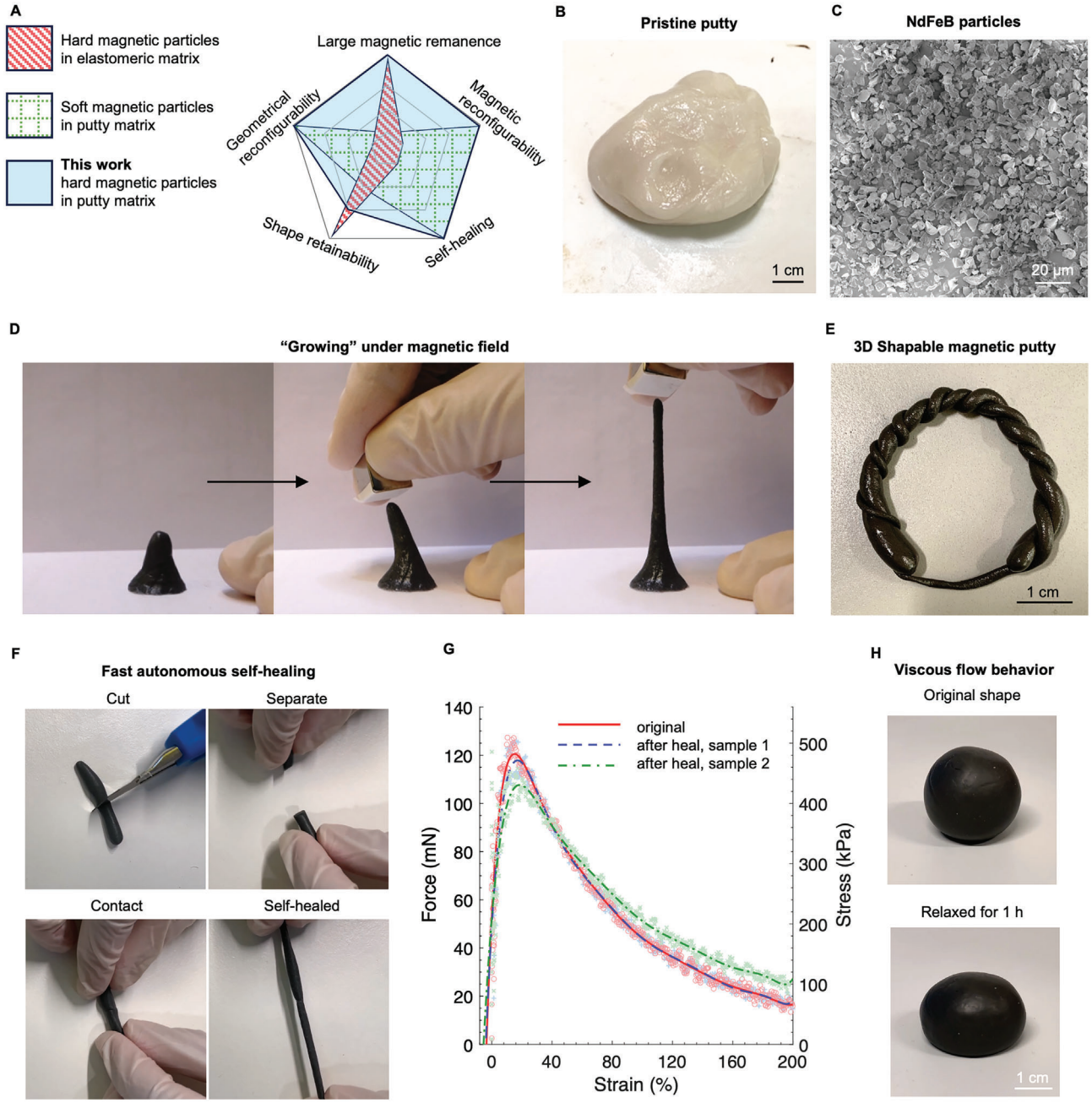


Figure 1. Magnetic putty composition, 3D shaping, and self-healing capabilities. A) Diagram comparing the key features of the magnetic putty in this work to other magnetic composites. B) Photo of the as-fabricated pristine putty. C) Scanning electron microscopic image of the Neodymium-Iron-Boron (NdFeB) microparticles used to mix with the pristine putty to make magnetic putties. D) Image sequence showing magnetic putty extending using a permanent magnet. E) An intertwined wreath made of magnetic putty. F) Image sequence showing the cutting and autonomous self-healing of magnetic putty based on contact. G) Force/stress versus strain curves of the original (control) sample and the two self-healed samples. A tenth-degree polynomial fitting was applied to smooth out the fluctuation and represent the trend of the raw data points. H) Shape relaxation of the magnetic putty when left undisturbed.

The magnetic putty shows thixotropic behavior: under a high shear strain such as during kneading, the moduli decrease, making the putty softer and malleable; under a small shear strain or left undisturbed, the putty self-stiffens, recovering its moduli over time (Figure 2C). The self-stiffening can last for over 48 h, with a ≈23-fold increase of storage modulus (Figure S4B, Supporting Information). As shown in Figure S4C (Supporting Information), pristine putty shows less than a 10% increase in its complex viscosity ($\Delta\eta^*/\eta_o^*$, while $\eta^* = G^*/\omega$), which can be attributed to dynamic bond reforming and polymeric chains entangling. The self-stiffening is enhanced after particle addition $\Delta\eta^*/\eta_o^*$ ≈40%). The greatest viscosity enhancement is achieved

© 2023 The Authors. Advanced Materials published by Wiley-VCH GmbH

15214095, 2023, 48, Downloaded from https://onlinelibrary.wiley.com/doi/10.1002/adma.202304825 by Koc University, Wiley Online Library on [26/02/2024]. See the Terms and Conditions (https://onlinelibrary.wiley.com/terms-and-conditions) on Wiley Online Library for rules of use; OA articles are governed by the applicable Creative Commons License

15214095, 2023, 48, Downloaded from https://onlinelibrary.wiley.com/doi/10.1002/adma.202304825 by Koc University, Wiley Online Library on [26/02/2024]. See the Terms and Conditions (https://onlinelibrary.wiley.com/terms-and-conditions) on Wiley Online Library for rules of use; OA articles are governed by the applicable Creative Commons License

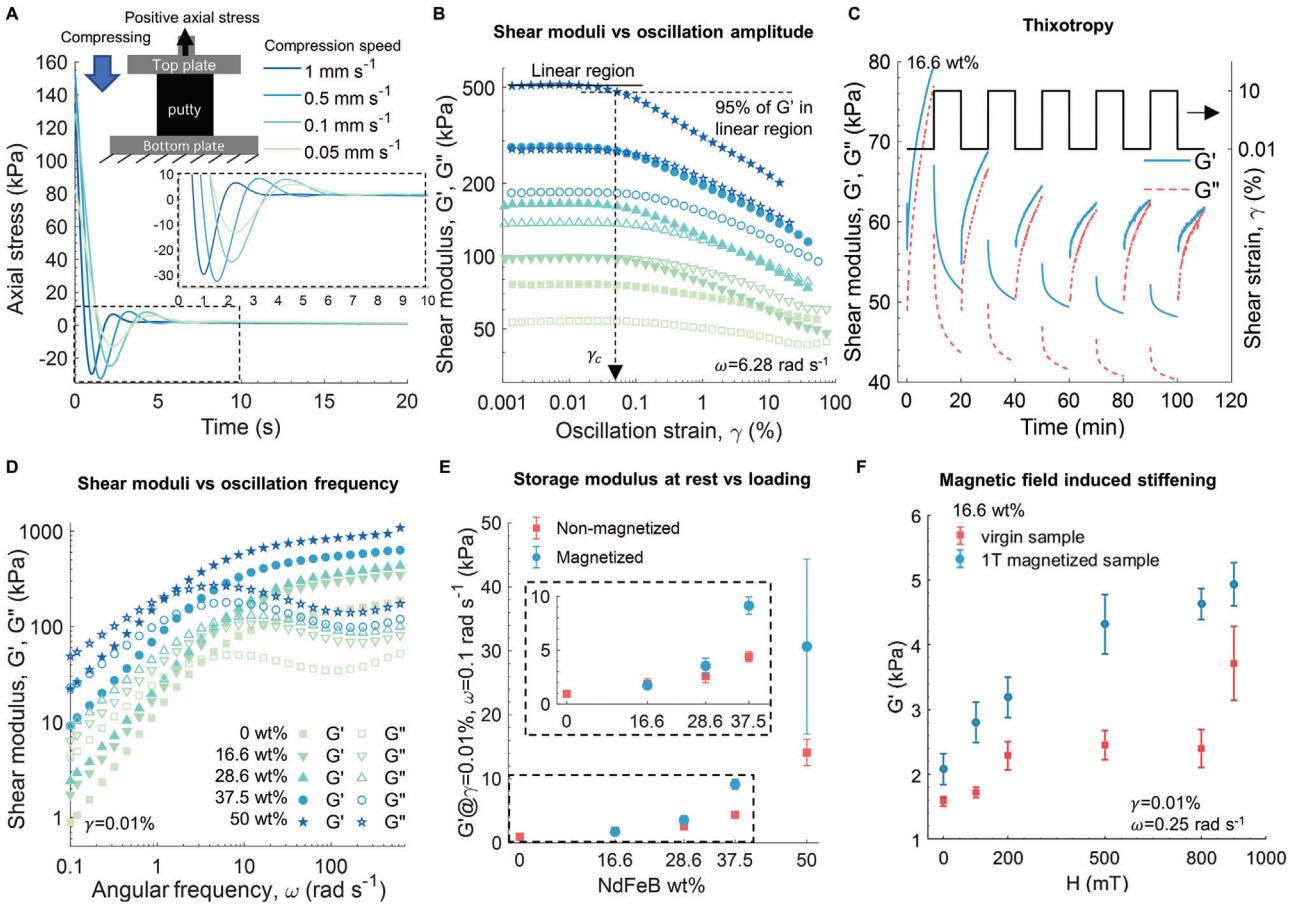


Figure 2. Rheological characterization of the magnetic putty. A) Squeeze-flow compression of 16.6 wt.% magnetic putty between two parallel plates at different compression rates. The time 0 marks when the top plate stops moving downward. The axial stress exerted on the top plate dampens and relaxes. The dash line-enclosed area is enlarged closer look of the time frame 0–10 s. B) Shear moduli measurements of magnetized putty samples and pristine putty during oscillation amplitude sweeping while keeping the oscillation frequency ω constant at 6.28 rad s^{-1} (1 Hz). Figure legend is the same as in panel D. C) Shear moduli of 16.6 wt.% magnetic putty measured with 0.01–10% alternating strain switched every 10 min. The oscillation frequency ω is kept at 6.28 rad s^{-1}. D) Shear moduli measurements of magnetized putty samples and pristine putty during oscillation frequency sweeping while keeping the oscillation strain amplitude γ constant at 0.01%. E) Storage modulus of 1.8 T-magnetized and non-magnetized putty with different NdFeB loadings at 0.01% strain and 0.1 rad s^{-1} frequency. Error bars represent ±standard deviation of three measurements. F) Storage modulus of 16.6 wt.% non-magnetized and 1 T-magnetized magnetic putty samples at 0.01% strain and 0.25 rad s^{-1} frequency under homogeneous magnetic fields of various magnitudes in the axial direction. Error bars represent ±standard deviation of three measurements.

when the magnetic particles are magnetized ($\Delta\eta^*/\eta_o^* \approx 180\%$) since magnetized particles in proximity can aggregate over time to form larger clusters due to dipole–dipole interactions.

During the frequency-sweeping measurements, the oscillation strain amplitude is kept constant at the value chosen from the linear viscoelastic region determined from the amplitude-sweeping measurements to avoid putty yielding. The magnetic putty has a larger storage modulus than loss modulus at higher shear rates (Figure 2D), indicating a more elastic behavior at time scales that are quicker than the speed of bonds breaking and reforming. At low shear rates, the putty is given enough time to reform those dynamic crosslinks, and the mechanical energy is largely dissipated within the matrix. In summary, the larger the shear rate is, the higher the storage modulus is, the more solid-like the putty behaves, and the lower viscosity the putty shows (Figure S5, Supporting Information). The putty also undergoes softening at increased temperatures due to increased mobility of the polymeric chains and the breakage of temporary crosslinks;[29] for 44.4 wt.% magnetic putty, G' gradually changed from 460 to 70 kPa as temperature increased from 20 to 90 °C (Figure S6, Supporting Information). This feature could be used to temporarily increase the deformation capability of magnetic putty using heat (either directly or wirelessly using light for instance) when it needs to travel through a tight space.

Magnetic putties with magnetized particles have higher shear moduli than the non-magnetized ones due to increased magnetic interactions among the particles, especially at higher particle loadings (Figure 2E; Figure S7, Supporting Information). Particle magnetization increases with increasing magnetic field; the increase is especially prominent for virgin (non-magnetized) samples (Figure S8G, Supporting Information). Under the same magnetic field, magnetized samples have a larger storage modulus than virgin samples. Due to the increased dipole–dipole interactions between particles of increased magnetization, the

 © 2023 The Authors. Advanced Materials published by Wiley-VCH GmbH

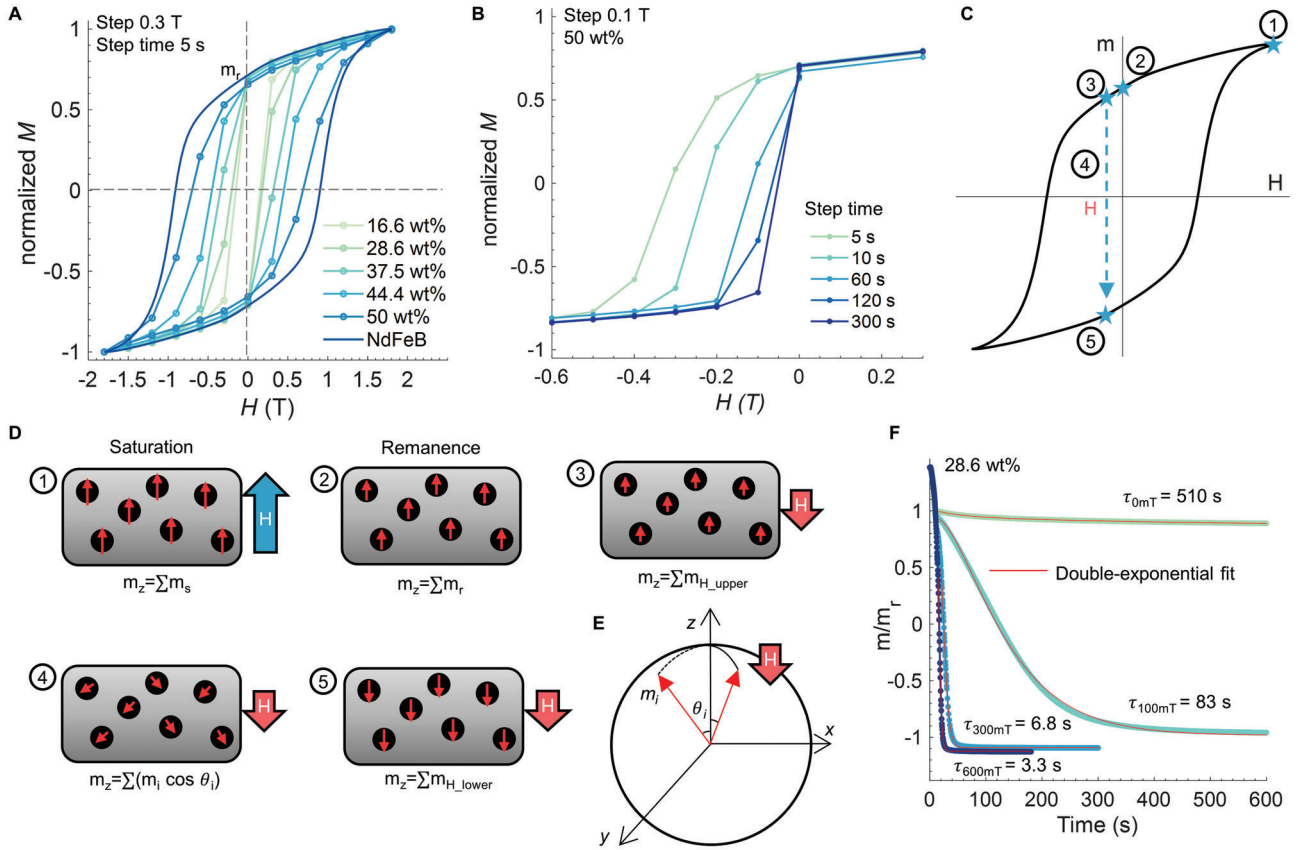


Figure 3. Magnetic characterization of the magnetic putty. A) Hysteresis loops of NdFeB particles and magnetic putty with different particle loadings. The external field changes at a step size of 0.3 T and the waiting time at each magnetic field point is 5 s. The curves are normalized by dividing the maximum magnetic moment value obtained under 1.8 T. B) The upper hysteresis loops of 50 wt.% putty sample in the range of 0.2 to −0.6 T with different waiting times between each data point. The external field is decreased by a step size of 0.1 T. The curves are normalized in the same way as panel A. C) Hysteresis loop of NdFeB particles to show different stages of putty magnetization. D) Simplified schematic showing how the particle physically rotates at different stages of the hysteresis measurements. The numbering matches those marked in panel C. E) Definition of the coordination system of magnetic field direction $-z$, particle magnetic moment m_i, and the angle θ_i between m_i and direction z. F) Relaxation of magnetic moment of 28.6 wt.% magnetic putty under reversal magnetic fields. The putty is first subject to a positive z-direction 1.8 T for 10 s. The time 0 marks when the field in the negative z-direction is applied. The solid-red lines are fitting curves using a double-exponential equation which gives time constant values τ.

putty shows magnetically induced stiffening (Figure 2F; Figure S8, Supporting Information). Under a 0.5 T magnetic field, magnetized putty shows a twofold G' increase and a virgin sample fourfold. The magnetorheological effect is not as prominent as ferrofluid which can have more than tens of thousands of folds of moduli enhancement due to the larger baseline storage moduli (under no magnetic field) the magnetic putty has. Nevertheless, one could use this feature of the magnetic putty in various applications, such as contactless change of load-bearing capability, vibration damping, and mechanical wave propagation, among others.

2.3. Magnetic Properties: High Remanence with Small Coercivity

The viscoelastic and the unbinding nature of the silicone putty matrix give the magnetic putty its unique magnetic properties: not only the magnetization magnitude of the putty but also the coercivity is dependent on the particle loading. Under the same measuring parameters, the magnetization direction of less-loaded magnetic putties can be reversed upon the application of a smaller external field (**Figure 3**A). All magnetic putty samples have a smaller apparent coercivity than the magnetic filler particles (NdFeB) at 1 T, with the upper first and lower third quadrants of the hysteresis loops overlapping. A longer waiting time between measuring points also gives a smaller apparent coercivity (Figure 3B); when applied for 300 s, 100 mT is enough to fully remagnetize the sample along the opposite direction.

The particle-loading and time dependence of the putty coercivity is due to the physical rotation of the magnetized particles in the soft and unbinding putty matrices.[36,37] The less the particle loading is, the softer the matrix is (as shown in Figure 2E), thus the faster the particles can rotate in the matrix under magnetic torque, which leads to a smaller apparent coercivity. In other words, the magnetic hardness of the magnetic putty is coupled with its mechanical stiffness.

NdFeB particles have irregular shapes composed of many nanograins with magnetic easy axes,[38] but here we can use a simplified model to describe the magnetization reversal process

© 2023 The Authors. Advanced Materials published by Wiley-VCH GmbH

15214095, 2023, 48, Downloaded from https://onlinelibrary.wiley.com/doi/10.1002/adma.202304825 by Koc University, Wiley Online Library on [26/02/2024]. See the Terms and Conditions (https://onlinelibrary.wiley.com/terms-and-conditions) on Wiley Online Library for rules of use; OA articles are governed by the applicable Creative Commons License

15214095, 2023, 48, Downloaded from https://onlinelibrary.wiley.com/doi/10.1002/adma.202304825 by Koc University, Wiley Online Library on [26/02/2024]. See the Terms and Conditions (https://onlinelibrary.wiley.com/terms-and-conditions) on Wiley Online Library for rules of use; OA articles are governed by the applicable Creative Commons License

by treating each magnetic particle as a single-domain magnetic moment. When one applies a saturating magnetic field in the z-direction (step 1 in Figure 3C,D), every magnetic particle has a saturated magnetic moment (m_s) and the net magnetic moment of the putty in this direction (m_z) is the sum of m_s of all particles. After removing the external magnetic field (step 2), all the particles are left with a remanent magnetic moment (m_r) and so is the putty. When a small field in the opposite direction is applied, almost instantaneously, the particle magnetization is slightly reduced from m_r, following the hysteresis curve of the particles (step 3). Since the particles are mobile in the soft putty matrix, under the magnetic torque, they will immediately start rotating to align their magnetic moments with the direction of the external field, which is the negative z-direction in this case (step 4). During this transition, the measured m_z is the sum of the z-component of magnetic moments from all particles (Figure 3E). During this rotation process, m_z is an exponential function of time (Figure 3F) with a time constant proportional to $\eta/(MH)$,[39] where η is the viscosity of the matrix, M is the magnetization of each particle and H is the reversal field strength. The larger the reversing field is, the faster the magnetic particles rotate, and the less time it takes for the putty to be remagnetized. When all magnetized particles are fully oriented along the negative z-direction, the putty m_z corresponds to the sum of particle magnetic moment at the lower side of the hysteresis loop (step 5).

Magnetic putty as a composite material has large remanence—equal to its hard-magnetic particle filler—enabling large magnetic response even under small external fields. At the same time, it shows low coercivity so that it can be remagnetized with an accessible small field provided by permanent magnets or custom-made electromagnetic coils. Furthermore, the particle-rotation introduced remagnetization does not just bring the net magnetization to the opposite direction, but also with maximum magnitude, creating a vertical "shortcut" on the hysteresis loop from one end to the other.

2.4. Putty Magnetization and Its Retention

By kneading the putty, one can demagnetize it by randomizing the orientation of the magnetized particles. To make it useful as a hard-magnetic material, one needs to endow it with magnetization along a desired direction and preferably also with a desired magnitude. While primary magnetization refers to the magnetization process of the magnetic particles by exposing the magnetic putty to a large magnetic field (e.g., 1.8 T in our case), secondary magnetization refers to putty magnetization resulting from aligning the magnetic moments of each magnetized particle without changing their magnetization.[40] The particles in the putty matrix are subject to randomizing forces even when left undisturbed. The secondary magnetization is a result of particles rotating in the putty matrix under magnetic torque and fighting against the randomizing forces. Thus, the magnetic field strength plays a determining role in the magnetization speed and magnitude. As pictured in **Figure 4**A, only with large enough magnetic torque, the particles can fully overcome the randomization force and the putty can be magnetized maximally (achieve unidirectional alignment of all the particle magnetic moments along with the external magnetic field). The putty magnetic moment in the direction of the external field increases over time and eventually plateaus (Figure 4B). For the 16.6 wt.% magnetic putty that is rested for 3 h before testing (slightly stiffer than the freshly kneaded one but gives more repeatable results), the threshold strength of the external field to achieve full magnetization ($m/m_r = 1$) is 120 mT (Figure 4C). The stiffer the magnetic putty is, the higher this threshold is. For instance, for 50 wt.% putty, the threshold is larger than 150 mT (Figure S9, Supporting Information). The randomizing energy is estimated to be on the order of 10^{-14} J (Figure S10, Supporting Information), which is multiple orders larger than the thermal energy k_BT at room temperature ($\approx 4 \times 10^{-21}$ J), indicating the randomization of the particle orientations is caused by other than mere thermal fluctuation.

We have shown that the magnetic putty can be remagnetized using a much smaller field (≈100 mT) than the coercivity of the filler particles (≈1 T). The next question is how well the magnetization retains after the magnetizing field is removed. We first magnetized the magnetic putty samples fully by applying a magnetic field above the threshold strength for a long enough period to bring m/m_r to 1. Then, we removed the external magnetic field and measured the relaxation of the putty magnetic moment (Figure 4D). A stiffer magnetic putty retards the particle rotation thus slowing down the magnetic relaxation. For example, for freshly-kneaded 16.6 wt.% magnetic putty, the relaxation time constant τ is fitted to be ≈60 s, while for a 1-hour rested 28.6 wt.% sample it is ≈500 s (as shown in Figure 3F for 0 mT reversing field). Also, magnetic particles aggregate to form larger particles after being magnetized due to magnetic interaction. Using an idealized model where all particles are spherical with the same size,[40] τ equals $1/(2D)$, where D is the diffusion constant which is reversely proportional to the constant of resistance for rotational motion in a viscous media, that is, $D \propto 1/\nu$ and $\nu \propto r^3\eta$. With particle size increasing, diffusion constant decreases dramatically and relaxation time constant increases, meaning a more stable magnetization over time.

Besides putty stiffness, we observed that the strength of the magnetizing field and the magnetizing duration (t_{mag}) also affect the magnetization retention (Figure 4D). When a larger magnetic field is applied (such as 1.8 T in this case), the particles are more likely to form chains (Figure S11, Supporting Information); a chain geometry increases the resistance of rotation in the putty, thus favoring less magnetic relaxation. For all three magnetizing field strengths we evaluated, we observed an increasing trend in magnetization retention as t_{mag} increases as shown in Figure 4E. On one hand, the longer the field is applied, the particles are given more time to travel within the putty to form larger aggregations. But for a small magnetizing field (e.g., 100 mT), when the chain formation is less significant, the trend is still present. We attribute this extra loss of retention with short t_{mag} to the elastic recoil of the putty matrix.[39] When the particles rotate during the secondary magnetization, the surrounding matrix deforms from this rotational shear as depicted in Figure 4F. The putty matrix is viscoelastic; while the orientation of the particles is pinned in place under the magnetizing field, the stress at the interface of the twisted matrix and the particles can relax. But if the field is removed before this stress is fully relaxed, the matrix recoils and exacerbates the randomization of the particles.

© 2023 The Authors. Advanced Materials published by Wiley-VCH GmbH

15214095, 2023, 48, Downloaded from https://onlinelibrary.wiley.com/doi/10.1002/adma.202304825 by Koc University, Wiley Online Library on [26/02/2024]. See the Terms and Conditions (https://onlinelibrary.wiley.com/terms-and-conditions) on Wiley Online Library for rules of use; OA articles are governed by the applicable Creative Commons License

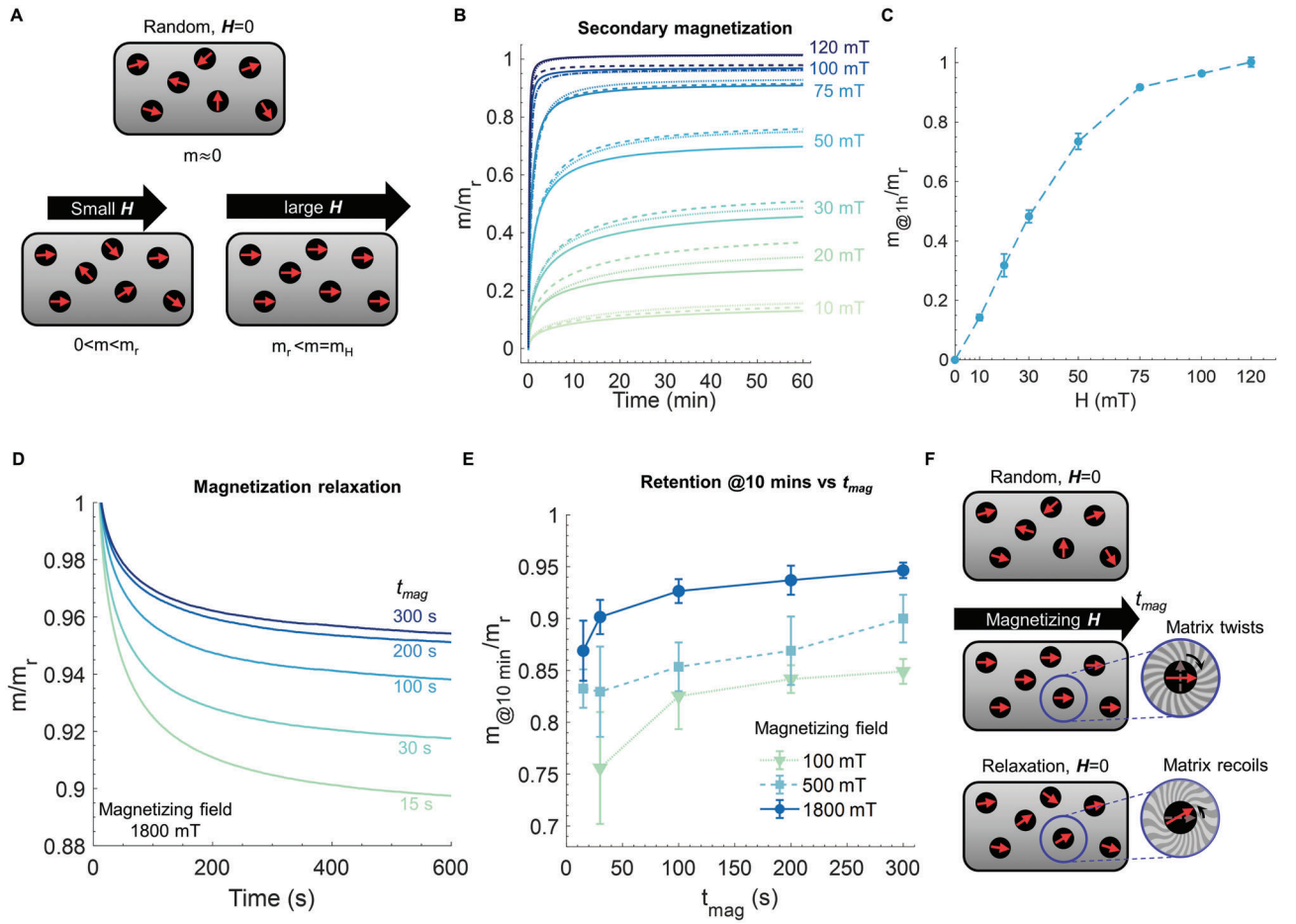


Figure 4. Secondary magnetization and magnetization retention of the magnetic putty. A) Simplified schematic showing how randomly-orientated particles align under external magnetic fields. B) The normalized magnetization of 16.6 wt.% putty over time during the secondary magnetization under different magnetizing fields. The curves are normalized by dividing the remanent magnetic moment measured for each sample. For each magnetizing field, three measurements are repeated and plotted in the figure. The putty is rested for 3 h and time 0 marks when the magnetizing field is applied. C) Normalized magnetization of 16.6 wt.% putty at 1 h of magnetic field application with different magnetizing field amplitudes. Error bars are ±standard deviation of three measurements. D) Normalized magnetization relaxation of 16.6 wt.% putty after applying a 1.8 T magnetizing field for various durations t_{mag}. Time 0 marks when the magnetizing field is removed. E) Normalized magnetization retention of 16.6 wt.% putty after 10-minute relaxation after applying various magnetizing fields for various durations t_{mag}. Error bars are the ±standard deviation of three measurements. F) Simplified schematic showing the matrix twisting during the magnetization process and the matrix recoiling after the removal of the field.

If good magnetization retention is desired, it is better to use a larger magnetizing field for a longer period during the secondary magnetization.

2.5. Magnetomechanical Responses

Many works have been conducted on the modeling of magneto-mechanical properties of soft materials embedded with hard-magnetic particles.[41–44] Due to the time-dependent magnetization change shown in previous sections, we anticipate that the magneto-mechanical response of the magnetic putty system is unique, especially under alternating magnetic fields. Starting with a static field, randomized magnetic putty was pressed in between two parallel plates, and a uniform static (DC) magnetic field was applied. The stress exerted on the top plate was recorded and plotted in **Figure 5**A. Regardless of the field direction, the field-induced stress is always positive due to the magnetostrictive effect; the putty would expand if it were not constrained between the two plates, which will exert positive stress on the top plate regardless of the field direction.

When we applied a slowly oscillating magnetic field in the axial direction (Figure S12, Supporting Information), we observed that the stress and shear moduli minimum occur after the magnetic field crosses zero. In previous sections, we have shown that when the field is reversed, the putty magnetization is slowly reduced first to zero and then reversed. When the magnetization in the axial direction is reduced to zero, the average orientation of the particle chains and the particle–particle interactions are in the lateral direction, which contributes the least to the axial volume expansion thus giving an axial stress minimum after the magnetic field switches direction.

Magnetic putty distinguishes itself from other magnetic soft materials in terms of its time-dependent magnetization in

© 2023 The Authors. Advanced Materials published by Wiley-VCH GmbH

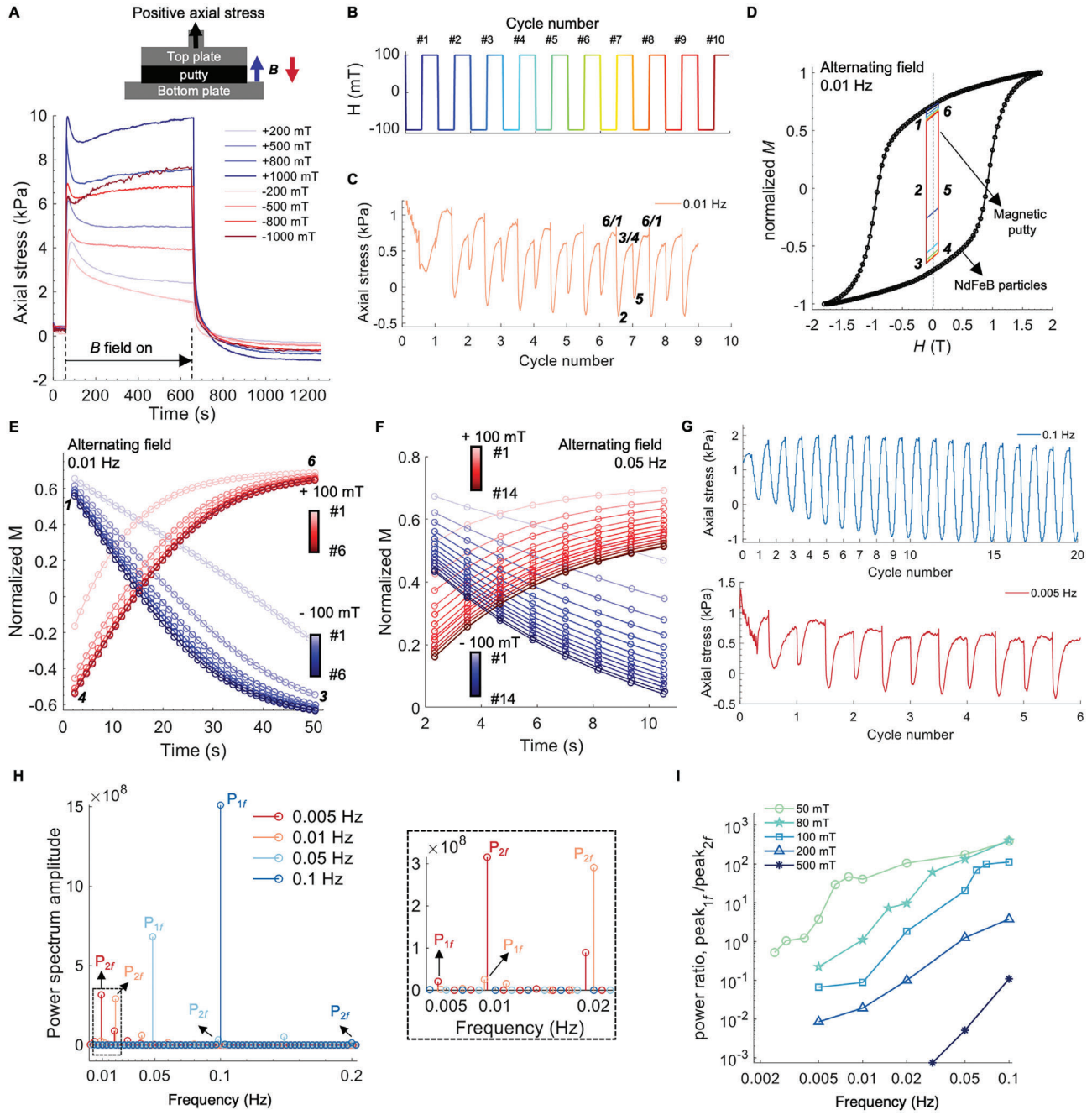


Figure 5. Magnetomechanical responses of the magnetic putty. A) 28.6 wt.% putty fixed between two parallel plates exerts axial stress upon the application of a homogeneous magnetic field of various magnitudes in the axial direction. Upward direction is defined as positive. B) Homogeneous magnetic field applied as a square wave with an amplitude of 100 mT. C) The axial stress of 16.6 wt.% putty plotted as a function of the magnetic field cycle number. The magnetic frequency is 0.01 Hz. D) Normalized magnetization of the 16.6 wt.% putty during the application of the 0.01 Hz magnetic field square wave. The color is consistent with that in panel B for each magnetic field cycle. The hysteresis loop of NdFeB particles is plotted as a reference. E) Normalized magnetization of the 16.6 wt.% putty plotted as a function of time during each magnetic cycle. Magnetic frequency is 0.01 Hz. The bold numberings match those in panel C and D to show different stages of the magnetization change and axial stress change. F) Normalized magnetization of the 16.6 wt.% putty plotted as a function of time during each magnetic cycle. Magnetic frequency is 0.05 Hz. G) Axial stress of 16.6 wt.% putty plotted as a function of the magnetic field cycle numbers which has an amplitude of 100 mT and a frequency of 0.1 and 0.005 Hz. H) The power spectrum amplitude obtained by fast Fourier transformation of the axial stress data of 16.6 wt.% magnetic putty. The single-frequency peak (P_{1f}) and the doubled-frequency peak (P_{2f}) mark the peak positions at the single and double frequency of the applied magnetic field frequency. For example, if the magnetic field alternates at 0.05 Hz, P_{1f} indicates the peak position at 0.05 Hz while P_{2f} is at 0.1 Hz. The dashed area is enlarged, showing a closer look at the low frequency range between 0.005–0.02 Hz. I) The power ratio of the single and double frequency peaks plotted as a function of the magnetic field frequency for various field amplitudes.

© 2023 The Authors. Advanced Materials published by Wiley-VCH GmbH

15214095, 2023, 48, Downloaded from https://onlinelibrary.wiley.com/doi/10.1002/adma.202304825 by Koc University, Wiley Online Library on [26/02/2024]. See the Terms and Conditions (https://onlinelibrary.wiley.com/terms-and-conditions) on Wiley Online Library for rules of use; OA articles are governed by the applicable Creative Commons License

response to external magnetic fields. Thus, we can use static magnetic fields to decouple the influence of external magnetic fields to study how magnetization affects magnetostrictive properties. Since the particle rotation is time-dependent, the frequency of the external magnetic field will affect the magnetization change of the magnetic putty and shape the magneto-mechanical response. We applied a square wave magnetic field with an amplitude of 100 mT to a fully magnetized putty sample (Figure 5B). When the alternating frequency is 0.01 Hz (the field switches direction every 50 s), the axial stress curve shows two peaks within each cycle (Figure 5C). We can map the measured stress response to the magnetization response measured separately using a vibrating sample magnetometer (VSM) (see Figure 5D,E). We noticed that it took three cycles for the magnetization loop to stabilize. Despite being embedded with hard-magnetic particles with a wide hysteresis loop, the composite system overall can operate at a much narrower hysteresis loop with a large magnetization magnitude. At a higher frequency, within each step, there is not enough time for the particles to be fully reversed before the magnetic field switches direction. It takes more cycles to stabilize the magnetization and the stabilized magnetization loop does not reach the full magnitude (Figure 5F; Figure S13B, Supporting Information). At a lower frequency, when the particles have enough time to be fully aligned in each step, the magnetization response is stabilized after only one cycle, and the range is maximized (Figure S13C,D, Supporting Information). Under an alternating magnetic field, the stress oscillates at a frequency that is modulated by the field frequency. As shown in Figure 5G, at a relatively high frequency (0.1 Hz), the axial stress oscillates at the same frequency as the magnetic field; however, at a low frequency, for example, 0.005 Hz, the stress peak occurs twice within each cycle, so the output (stress) frequency doubles that of the input (magnetic field). The fast Fourier transformation of the stress–time curve (Figure 5H) quantitatively shows that a larger magnetic field strength and a lower magnetic field frequency reverse putty magnetization more effectively with a bigger proportion of the doubled-frequency component. By changing the frequency and/or amplitude of the input alternating magnetic field, one can modulate the frequency components of the output signal which is manifested as the axial stress from magnetic putty constrained between two plates (Figure 5I). The characterized frequency-dependent magneto-mechanical response could provide guidance to the design of dynamic magnetic robots. For example, by combining two pieces of magnetic putties with different response times together, at short time frames, the geometrically symmetric actuator will deform asymmetrically; over a long period of time, both pieces are fully remagnetized thus the symmetricity is resumed.

2.6. Applications of Magnetic Putty

2.6.1. Reconfigurable Magnetic Setups

Electromagnetic coils and permanent magnet arrays are two commonly used setups for small-scale magnetic robots. Permanent magnet arrays provide an always-on magnetic field pattern. By arranging the magnets in specific locations and orientations, one can generate specific magnetic field patterns. For example, dipole Halbach cylinders generate a uniform field along one radial direction,[45,46] Aubert ring pairs along the axial direction,[47] and an optimized five-ring configuration can create a force trap in the center of a 3D workspace.[48] Making one of these arrays using permanent magnets is limited by the geometry of commercially available magnets and once it is constructed, the generated magnetic profile is fixed. We propose here using magnetic putty as a filler material, which can be used with holders of nonspecific shapes. More importantly, the magnetization profile can be easily reconfigured (**Figure 6**A). Using the same holder and same magnetic putty, we constructed a dipole Halbach array that generates a uniform 25 mT in the desired direction (Figure 6B) and later we changed it into a quadrupole Halbach array that has zero fields in the center but provides magnetic field gradients (Figure 6C; Figure S14, Supporting Information). The reconfiguration was done by remagnetizing and rearranging some of the modules. This quickly-built and easily reconfigurable magnetic setup can be used to test magnetic soft robots (Movie S5, Supporting Information).

2.6.2. Shapable Magnet with Adaptive Magnetic Polarities

The putty can be easily formed into 3D shapes and largely maintain those shapes. It can also be used as a filler or attached to arbitrary surfaces, rendering inert objects magnetically responsive. Once fully magnetized, it can provide strong magnetic interactions. Unlike a permanent magnet, the polarity of a putty magnet can adapt to external fields without physically re-orienting (Figure 6D). Thus, the putty is attracted to a magnet regardless of its orientation and the polarity of the magnet, showing magnetic adaptivity (Movie S6, Supporting Information). This feature can be used to provide safety retrieval of hard-magnetic robots, especially in hard-to-access in vivo areas, when the physical orientation of the robots is limited, and imaging and physical contact are not feasible.

2.6.3. Recyclable Material for Fast Prototyping

Magnetic soft robots are commonly made of elastomers doped with magnetic fillers, whose fabrication process usually involves mixing, degassing, curing, shaping, and assembling (Figure S15, Supporting Information). Using the magnetic putty, one can directly start shaping it to the desired 3D geometries and magnetize each segment with a relatively small field (200 mT compared with 1 T), which can be sufficiently generated from an easier-to-access permanent magnet. The segments can be readily joined together without extra adhesive. As shown in Figure 6E, we assembled a crawling robot with 8 pieces of magnetic putty sheets of various magnetization directions. Under an out-of-plane rotating magnetic field, the robot can locomote using pedal motion and body modulation (Figure 6F, Movie S7, Supporting Information). The same putty can be recycled and reused by kneading without material deterioration or degradation to fast prototype other robotic designs (Figure S16, Supporting Information). Thin backings can be used if the magnetic putty is too soft to support the structure. Because of the slight stickiness of the putty, it can be easily adhered to substrates, such as polymer films, papers, and metals.

© 2023 The Authors. Advanced Materials published by Wiley-VCH GmbH

15214095, 2023, 48, Downloaded from https://onlinelibrary.wiley.com/doi/10.1002/adma.202304825 by Koc University, Wiley Online Library on [26/02/2024]. See the Terms and Conditions (https://onlinelibrary.wiley.com/terms-and-conditions) on Wiley Online Library for rules of use; OA articles are governed by the applicable Creative Commons License

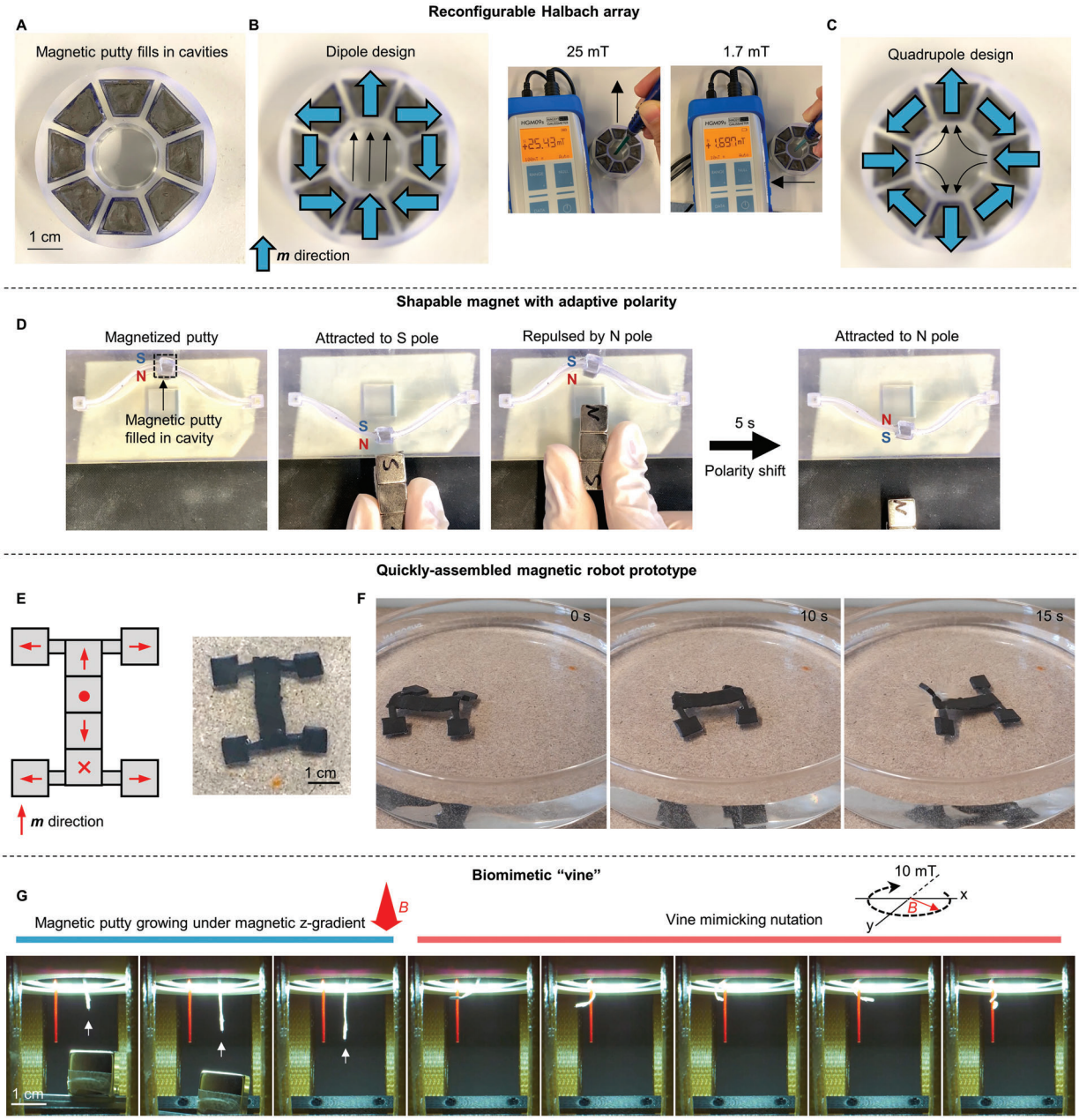


Figure 6. Application demonstrations of the magnetic putty as a recyclable robotic material. A) Modular design of a 3D-printed Halbach cylinder with an inner diameter of 2 cm, an outer diameter of 5 cm, and a thickness of 2 cm. Each of the eight cavities can be removed from the holder, filled with 50 wt.% magnetic putty, and magnetized individually. B) Halbach array dipole design. Each section is magnetized as indicated by the blue arrow to generate a homogeneous magnetic field in the direction indicated by the black arrow arrays in the central working area. Magnetic field strength is measured in the center in two orthogonal directions that are marked with arrows. C) Halbach array quadrupole design to generate a magnetic field gradient in the central working area. The magnetic flux directions are indicated by the black arrows. D) Adaptive polarity of magnetic putty. The magnetic putty was filled in a cavity in the center of a bi-stable beam. E) Design schematic and photo of the magnetic walker, quickly fabricated by assembling magnetic putty patches with the marked magnetization directions. F) Photo sequence of magnetic walker locomote in water under an out-of-plane rotating magnetic field. G) Demonstration of using magnetic putty to mimic the growing and nutational motion of twining plants. White arrows mark the position of the growing magnetic putty.

2.6.4. Bioinspired "Vine" with Contactless Controls

Inspired by the growing and dramatic nutational motion of searcher twigs of lianas, such as cardinal climber and morning glory, we used magnetic putty to mimic these motions with contactless controls (Movie S8, Supporting Information). As shown in Figure 6G, under a magnetic gradient in the *z*-direction, the putty was elongated showing a growing effect. More importantly, the magnetization direction was aligned along the growing direction and maintained after the

© 2023 The Authors. Advanced Materials published by Wiley-VCH GmbH

15214095, 2023, 48, Downloaded from https://onlinelibrary.wiley.com/doi/10.1002/adma.202304825 by Koc University, Wiley Online Library on [26/02/2024]. See the Terms and Conditions (https://onlinelibrary.wiley.com/terms-and-conditions) on Wiley Online Library for rules of use; OA articles are governed by the applicable Creative Commons License

magnet was removed, making programmed magnetic actuation possible. Using a 10 mT rotating magnetic field in the *xy*-direction, the putty "vine" was lifted under the magnetic torque and the vine tip followed the rotation and wrapped around a nearby pole, mimicking the nutational motion of natural vines.

3. Conclusion

This paper introduces magnetic putty as a versatile soft magnetic robotic material that can be easily reconfigured both geometrically and magnetically. The composite material is made of a viscoelastic soft putty matrix with embedded permanent magnetic microparticles. The putty is silicone oil-based; it is easy to use without staining and provides durability as it does not dry out in the air. It can be shaped and assembled with ease by bringing two parts into contact with no additional energy input. The magnetic force provided by a permanent magnet is strong enough to change the geometry of the magnetic putty, and after the magnetic force is removed, the deformed shape stays. Magnetic putty shows time- and field-dependent magnetic coercivity due to the physical rotation of the magnetized particles in the matrix.

For future studies, it would be interesting to further understand the interplay of the viscoelastic properties and the magnetic properties of this soft hard-magnetic composite using modeling and simulation together with experimental validation. The shear moduli depend on the shear rate, while the local shear rate is proportional to the particle rotating speed which is affected by the matrix shear moduli, external field, and interactions with neighboring particles. Also, particles can translate within the putty matrix to form chains, which will also affect how they physically rotate in the viscoelastic matrix under magnetic fields. Based on that, reverse design could be possible to fabricate magnetic putty with the optimized putty composition and particle size to achieve desired performance, either mechanically or magnetically.

As a robotic material, magnetic putty is easy to use. After fabrication, the magnetic putty only needs to be magnetized once. After kneading–which demagnetizes the putty without heat nor applying a magnetic field–one can remagnetize it to its remanence along any direction given an external magnetic field of ≈100 mT. With its low remagnetization field requirements, magnetic putty can be a versatile tool for those who want to reprogram hard-magnetic materials but do not have access to high-intensity magnetic fields. Because it is easy to change its magnetic profile and it can keep its magnetization, the magnetic putty can be used as shapable and recyclable magnets for actuating magnetic soft robots. Or it can be the robot itself with fast shaping, programming, and assembling processes. However, it is worth noting that due to the flow nature of the viscoelastic putty, the shape will relax over time, which could be critical for stand-alone geometries. By using it as a filler material or adhering it to a more rigid supporting structure, one could overcome this long-term instability of the magnetic putty.

The time-dependent magnetization change can be used to fabricate complex and dynamic magnetic actuation. The characterization and demonstration of magnetic putty in this work could provide a starting point for further explorations. We foresee magnetic putty being used as an easy-to-access material for research and educational purposes within the soft robotics community.

4. Experimental Section

Pristine Putty Preparation: PDMS oligomer (Sylgard 184, Dow Inc.) and boric acid powder were manually mixed at a weight ratio of 10:3. The mixture slurry was heated up in an aluminum container on a hotplate set at 300 °C. The slurry bubbled vigorously as the generated water boiled. The slurry was stirred at this temperature for about another hour. During this process, the white boric acid powder dissolved, the slurry became thicker, opaque, and eventually, the bubbling ceased. The hotplate was turned off and the putty was left to cool down. Later, one could scrape it off from the aluminum foil and knead it to shape.

Magnetic Putty Preparation: To make 50 wt.% magnetic putty, pristine putty (5 g), and an equal weight of NdFeB particles (average diameter 5 µm, MQFP-B, Magnequench) were added to a 50 mL-polypropylene centrifugal tube. Chloroform (30 mL) was added to the tube to dissolve the putty. The process was sped up by using a vortex mixer. Once the putty was fully dissolved, in a fume hood, the caps of the tubes were removed to allow the solvent to evaporate. During the evaporation process, the mixture was agitated with a vortex mixer, facilitating a homogeneous dispersion of the magnetic particles in the putty matrix while the solvent dried. Once the tubes appeared dry, one could scrape the magnetic putty off from the tube wall. To ensure the solvent was completely evaporated, the magnetic putty was kneaded and spread thinly on a 60 °C-hotplate surface and left in the fume hood overnight. Then the putty could be stored in ambient conditions without particular care. For other particle-loadings, the 50 wt.% magnetic putty was proportionally mixed with the pristine putty followed by kneading.

Compression Measurements: A hybrid rheometer (Discovery HR-30, TA Instruments) was used for all the mechanical tests, including rheological measurements, compression tests, and axial stress measurements. The putty could self-adhere to metal surfaces. When pressed between the stainless-steel upper plate (20 mm in diameter) and the bottom substrate of the rheometer, no extra fixation was needed to prevent wall slipping during shear and detachment during axial measurement. After loading, the sample was rested until the axial force reached zero before compression started. When applying a compressive strain by lowering the upper plate at a constant rate (0.05, 0.1, 0.5, and 1 mm s^{-1}), the force–gap (F–h) curves were recorded. The volume of the putty (V) being compressed was fixed to fully cover the surface area of the upper plate when the gap height was 1 mm. During compression, the surface area (A) was constantly changing as the height of the sample (gap between the two plates, h) was continuously decreasing. The stress (σ) was calculated using $F/A = F/(V/h)$. For samples with significant flowability, the compression measurement was also referred to as squeeze flow measurements.[49,50] At the low strain region ($\epsilon < 0.2$), the stress–strain (σ-ϵ) curve was fitted and extracted the compressive modulus from the fitted slop. The stress was continued to be monitored after the top plate stopped moving to show the stress relaxation of the magnetic putty.

Rheological Measurements: A stainless steel 20 mm-diameter parallel top plate was used. Putty samples were kneaded for a minute before being placed on the bottom plate. The putty volume was determined so that when pressed to a 1 mm gap height, the surface area covered the top plate. The top plate was lowered to a gap size of 1 mm at a speed of 50 µm s^{-1}, immediately followed by a 10 min dynamic resting at an angular frequency of 6.28 rad s^{-1} and amplitude of 0.01%. The frequency sweep measurements were done at frequencies ranging from high to low, in order to obtain as many data points as possible in a short period of time since magnetic putty was unstable, stiffening over time. When temperature control was needed, a Peltier bottom plate (Peltier Plate Accessory, TA Instruments) and a chiller system were employed.

Axial Stress Measurements with an Oscillating Magnetic Field: For applying magnetic fields, an electromagnetic coil (Magneto-Rheology Accessory, TA Instrument) was used together with an upper yoke to generate a homogeneous magnetic field in the axial direction. Since the magnetic coil could significantly heat up during operation, chiller and coolant circulation was used to keep the sample at 20 °C. The putty was pressed to 1 mm height, followed by a 10-minute sample conditioning with an 800 mT magnetic field to bring particle alignment to the z-direction. Axial stress

© 2023 The Authors. Advanced Materials published by Wiley-VCH GmbH

15214095, 2023, 48, Downloaded from https://onlinelibrary.wiley.com/doi/10.1002/adma.202304825 by Koc University, Wiley Online Library on [26/02/2024]. See the Terms and Conditions (https://onlinelibrary.wiley.com/terms-and-conditions) on Wiley Online Library for rules of use; OA articles are governed by the applicable Creative Commons License

was recorded during the application of oscillating magnetic fields (either sine wave or square wave). A Hall probe was located directly beneath the sample to provide a closed-loop control of the magnetic field. It was noticed that when the oscillating frequency was set to be higher than 0.1 Hz, the actual magnetic field magnitude could not reach the set-amplitude.

Magnetic Moment Measurements: A VSM was used for all magnetic characterization. Magnetic putty was kneaded to demagnetize it. The magnetic putty was rolled in between two pieces of Parafilm into a 1 mm-thick sheet. Then using a pair of scissors, the sheet was cut into smaller pieces and attached to the VSM quartz rod sample holder. For the secondary magnetization, the putty was kneaded and rested for three hours before the measurements were begun. From the long-term shear moduli measurements, from 1- to 2 hours after kneading, the storage modulus was increased by 20%, while from 3- to 4 hours, the increase was only 5%. If no resting step was taken after kneading, the measurement was time-sensitive at a minute-scale, making it difficult to have repeatable results. For data normalization, immediately after the time sequence measurements $m(t)$, a hysteresis loop was measured to get the remanent magnetic moment for that sample. This way, it was not needed to precisely weigh each magnetic putty sample to calculate magnetization and we were still able to compare the degree of particle alignment m/m_r from sample to sample.

Supporting Information

Supporting Information is available from the Wiley Online Library or from the author.

Acknowledgements

The authors thank Scott A. Crooker, Jie Han, Zhen Yin, and Zhiqiang Zheng for the insightful discussions. M.L. thanks Anitha Shiva for the assistance of SEM imaging and Dan Skyer for the help with micro-CT imaging. M.L., J.B., and A.P. thank the Alexander von Humboldt Foundation for the sponsorship. G.G. thanks the International Max Planck Research School for Intelligent Systems for the financial support. M.S. thanks Max Planck Society and the European Research Council (Advanced Grant SoMMoR 834531) for the funding support.

Open access funding enabled and organized by Projekt DEAL.

Conflict of Interest

The authors declare no conflict of interest.

Data Availability Statement

The data that support the findings of this study are available from the corresponding author upon reasonable request.

Keywords

magnetic robots, reconfigurability, self-healing, soft matter, viscoelasticity

Received: May 22, 2023
Revised: August 31, 2023
Published online: October 25, 2023

[1] M. Li, A. Pal, A. Aghakhani, A. Pena-Francesch, M. Sitti, *Nat. Rev. Mater.* **2022**, *7*, 235.
[2] M. Sitti, *Nat. Rev. Mater.* **2018**, *3*, 74.
[3] F. Qiu, B. J. Nelson, *Engineering* **2015**, *1*, 021.
[4] M. Sitti, D. S. Wiersma, *Adv. Mater.* **2020**, *32*, 1906766.
[5] S. Miyashita, S. Guitron, S. Li, D. Rus, *Sci. Rob.* **2017**, *2*, aao4369.
[6] H. Gu, Q. Boehler, D. Ahmed, B. J. Nelson, *Sci. Rob.* **2019**, *4*, aax8977.
[7] G. Mao, M. Drack, M. Karami-Mosammam, D. Wirthl, T. Stockinger, R. Schwödiauer, M. Kaltenbrunner, *Sci. Adv.* **2020**, *6*, eabc0251.
[8] Y. Alapan, O. Yasa, O. Schauer, J. Giltinan, A. F. Tabak, V. Sourjik, M. Sitti, *Sci. Rob.* **2018**, *3*, eaar4423.
[9] V. Magdanz, I. S. M. Khalil, J. Simmchen, G. P. Furtado, S. Mohanty, J. Gebauer, H. Xu, A. Klingner, A. Aziz, M. Medina-Sánchez, O. G. Schmidt, S. Misra, *Sci. Adv.* **2020**, *6*, eaba5855.
[10] J. Cui, T.-Y. Huang, Z. Luo, P. Testa, H. Gu, X.-Z. Chen, B. J. Nelson, L. J. Heyderman, *Nature* **2019**, *575*, 164.
[11] U. Bozuyuk, E. Suadiye, A. Aghakhani, N. O. Dogan, J. Lazovic, M. E. Tiryaki, M. Schneider, A. C. Karacakol, S. O. Demir, G. Richter, M. Sitti, *Adv. Funct. Mater.* **2022**, *32*, 2109741.
[12] X. Yang, W. Shang, H. Lu, Y. Liu, L. Yang, R. Tan, X. Wu, Y. Shen, *Sci. Rob.* **2020**, *5*, abc8191.
[13] G. Z. Lum, Z. Ye, X. Dong, H. Marvi, O. Erin, W. Hu, M. Sitti, *Proc. Natl. Acad. Sci. U. S. A.* **2016**, *113*, E6007.
[14] Y. Kim, H. Yuk, R. Zhao, S. A. Chester, X. Zhao, *Nature* **2018**, *558*, 274.
[15] W. Hu, G. Z. Lum, M. Mastrangeli, M. Sitti, *Nature* **2018**, *554*, 81.
[16] S. Wu, W. Hu, Q. Ze, M. Sitti, R. Zhao, *Multifunct. Mater.* **2020**, *3*, 042003.
[17] T. Xu, J. Zhang, M. Salehizadeh, O. Onaizah, E. Diller, *Sci. Rob.* **2019**, *4*, eaav4494.
[18] Z. Liu, M. Li, X. Dong, Z. Ren, W. Hu, M. Sitti, *Nat. Commun.* **2022**, *13*, 2016.
[19] Y. Alapan, A. C. Karacakol, S. N. Guzelhan, I. Isik, M. Sitti, *Sci. Adv.* **2020**, *6*, eabc6414.
[20] H. Deng, K. Sattari, Y. Xie, P. Liao, Z. Yan, J. Lin, *Nat. Commun.* **2020**, *11*, 6325.
[21] X. Kuang, S. Wu, Q. Ze, L. Yue, Y.i Jin, S. M. Montgomery, F. Yang, H. J. Qi, R. Zhao, *Adv. Mater.* **2021**, *33*, 2102113.
[22] B. Mazzolai, A. Mondini, E. Del Dottore, L. Margheri, F. Carpi, K. Suzumori, M. Cianchetti, T. Speck, S. K. Smoukov, I. Burgert, T. Keplinger, G. D. F. Siqueira, F. Vanneste, O. Goury, C. Duriez, T. Nanayakkara, B. Vanderborght, J. Brancart, S. Terryn, S. I. Rich, R. Liu, K. Fukuda, T. Someya, M. Calisti, C. Laschi, W. Sun, G. Wang, L. Wen, R. Baines, S. K. Patiballa, et al., *Multifunct. Mater.* **2022**, *5*, 032001.
[23] A. Pena-Francesch, H. Jung, M. C. Demirel, M. Sitti, *Nat. Mater.* **2020**, *19*, 1230.
[24] S. Terryn, J. Brancart, D. Lefeber, G. Van Assche, B. Vanderborght, *Sci. Rob.* **2017**, *2*, eaan4268.
[25] M. Sun, C. Tian, L. Mao, X. Meng, X. Shen, B.o Hao, X. Wang, H. Xie, L.i Zhang, *Adv. Funct. Mater.* **2022**, *32*, 2112508.
[26] X. Fan, Y. Jiang, M. Li, Y. Zhang, C. Tian, L. Mao, H. Xie, L. Sun, Z. Yang, M. Sitti, *Sci. Adv.* **2022**, *8*, eabq1677.
[27] R. Baines, S. K. Patiballa, J. Booth, L. Ramirez, T. Sipple, A. Garcia, F. Fish, R. Kramer-Bottiglio, *Nature* **2022**, *610*, 283.
[28] E. Acome, S. K. Mitchell, T. G. Morrissey, M. B. Emmett, C. Benjamin, M. King, M. Radakovitz, C. Keplinger, *Science* **2018**, *359*, 61.
[29] V. D. Lobkov, A. L. Klebanskii, E. V. Kogan, *Polym. Sci. U. S. S. R.* **1965**, *7*, 1699.
[30] R. Weijermars, *Tectonophysics* **1986**, *124*, 325.
[31] T. I. Zatsepina, M. L. Brodskii, Y. A. Frolova, A. A. Trapeznikov, V. N. Gruber, G. A. Kruglova, *Polym. Sci. U. S. S. R.* **1970**, *12*, 2899.
[32] R. Cross, *Am. J. Phys.* **2012**, *80*, 870.
[33] F. Guo, C. Du, G. Yu, R. Li, *Adv. Mater. Sci. Eng.* **2016**, *2016*, e7079698.
[34] C. S. Boland, U. Khan, G. Ryan, S. Barwich, R. Charifou, A. Harvey, C. Backes, Z. Li, M. S. Ferreira, M. E. Möbius, R. J. Young, J. N. Coleman, *Science* **2016**, *354*, 1257.
[35] J. Yao, Y. Sun, Y. Wang, Q. Fu, Z. Xiong, Y. Liu, *Compos. Sci. Technol.* **2018**, *162*, 170.

© 2023 The Authors. Advanced Materials published by Wiley-VCH GmbH

15214095, 2023, 48, Downloaded from https://onlinelibrary.wiley.com/doi/10.1002/adma.202304825 by Koc University, Wiley Online Library on [26/02/2024]. See the Terms and Conditions (https://onlinelibrary.wiley.com/terms-and-conditions) on Wiley Online Library for rules of use; OA articles are governed by the applicable Creative Commons License

[36] G. V. Stepanov, A. V. Chertovich, E. Y. Kramarenko, *J. Magn. Magn. Mater.* **2012**, *324*, 3448.
[37] L. Cao, D. Yu, Z. Xia, H. Wan, C. Liu, T. Yin, Z. He, *Adv. Mater.* **2020**, *32*, 2000827.
[38] M. V. Vaganov, D. Y. Borin, S. Odenbach, Y. L. Raikher, *Soft Matter* **2019**, *15*, 4947.
[39] P. A. Valberg, J. P. Butler, *Biophys. J.* **1987**, *52*, 537.
[40] I. Nemoto, *IEEE Trans. Biomed. Eng.* **1982**, *BME-29*, 745.
[41] R. Zhang, S. Wu, Q. Ze, R. Zhao, *J. Appl. Mech.* **2020**, *87*, 091008.
[42] V. M. Kalita, A. A. Snarskii, D. Zorinets, M. Shamonin, *Phys. Rev. E* **2016**, *93*, 062503.
[43] D. Garcia-Gonzalez, M. Hossain, *EML* **2021**, *48*, 101382.
[44] T. A. Nadzharyan, M. Shamonin, E. Y. Kramarenko, *Polymers* **2022**, *14*, 4096.
[45] P. Blümler, Concepts in Magnetic Resonance Part B: Magnetic Resonance Engineering, Vol. *46* **2016**, 41-48.
[46] K. Halbach, *Nucl. Instrum. Methods* **1980**, *169*, 1.
[47] C. Hugon, P. M. Aguiar, G. Aubert, D. Sakellariou, *C. R. Chim.* **2010**, *13*, 388.
[48] D. Son, M. C. Ugurlu, M. Sitti, *Sci. Adv.* **2021**, *7*, eabi8932.
[49] N. Phan-Thien, R. I. Tanner, *J. Fluid Mech.* **1983**, *129*, 265.
[50] Y. Xu, X. Gong, T. Liu, S. Xuan, *J. Rheol.* **2014**, *58*, 659.

© 2023 The Authors. Advanced Materials published by Wiley-VCH GmbH

15214095, 2023, 48, Downloaded from https://onlinelibrary.wiley.com/doi/10.1002/adma.202304825 by Koc University, Wiley Online Library on [26/02/2024]. See the Terms and Conditions (https://onlinelibrary.wiley.com/terms-and-conditions) on Wiley Online Library for rules of use; OA articles are governed by the applicable Creative Commons License